Passive RADAR acoustic delay line sensor measurement: demonstration using a WiFi (2.4 GHz) emitter and WAIC-band (4.3 GHz)

Jean-Michel Friedt, Gwenhael Goavec-Merou, Gilles Martin
FEMTO-ST Time & Frequency, Besançon, France
Email: jmfriedt@femto-st.fr

Weike Feng, Motoyuki Sato
CNEAS, Tohoku University, Sendai, Japan
Email: feng.weike.q4@dc.tohoku.ac.jp

***Abstract*—We demonstrate passive RADAR interrogation of passive sensors: the non-cooperative signal source is analyzed to detect time-delayed copies of the reference signal generated by the cooperative target. The acoustic sensor is designed to introduce a delay dependent on a physical quantity under investigation, so that analyzing the echoes generated by the cooperative target allows for recovering the measured quantity. We demonstrate the passive RADAR principle for probing SAW cooperative targets acting as sensors using a WiFi emitter. Furthermore in the context of aeronautical deployment, we demonstrate the interrogation of a sensor operating in the 4.2–4.4 GHz WAIC (Wireless Avionics Intra-Communication) frequency band using a noise RADAR following principles similar to those implemented in a passive RADAR approach.**

I. Introduction

SAW transducers have emerged as an attractive solution for harsh environment sensing, whether addressing measurement challenges on moving parts in which no wires can be attached to (rotor), or environments too harsh for silicon-based electronics. However, unlike the RadioFrequency IDentification (RFID) industry, the passive wireless Surface Acoustic Wave (SAW) sensor industry has not been able to obtain the allocation of dedicated radiofrequency bands: short-range RADAR-like readers aim at fitting within existing radiofrequency emission regulations, making the certification challenging. Here we address the passive RADAR approach in which existing, non-cooperative emitters are used to probe a acoustic sensor.

Rather than using the magnitude of the echoes as indicators of sensor characteristics – prone to multiple artifacts including varying link budget and multipath interferences – we focus on precise time-of-flight identification through phase measurement. The first section deals with the measurement demonstration using a noise-RADAR, in which the carrier spectrum is spread using binary-phase shift keying modulation. Secondly, the dedicated emitter is replaced with a non-cooperative emitter, namely a commercial off the shelf 802.11 (WiFi) transceiver. The selection of the non-cooperative emitter to probe the wireless sensor must meet three criteria: spectrum matching between sensor and emitted signal both in carrier frequency and spectrum width, and sufficient power to compensate for the link budget decaying as the fourth power of the range. While WiFi meets the requirement of a 15 MHz bandwidth suitable for separating echoes delayed by more than 100 ns, 2.4 GHz carrier as found in multiple commercial SAW sensors, and power up to 20 dBm allowing for meter range bistatic range interrogation, we will improve the timing resolution by aggregating measurements collected in adjacent WiFi channels to increase the measurement bandwidth. A typical sensor response in the frequency and time domains is exhibited in Fig. 1: such a sensor will be used throughout these experiments.

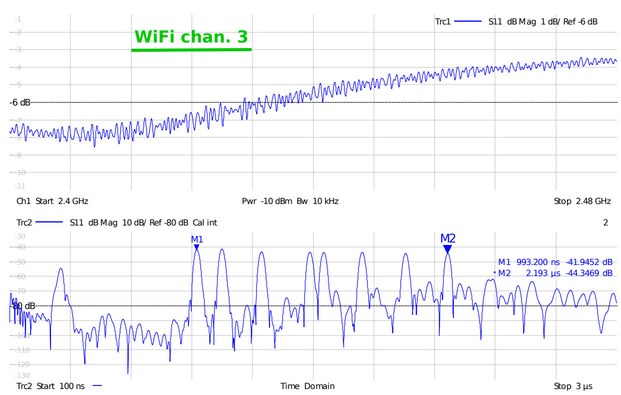

Fig. 1. Characterization of a 2.4 GHz delay line provided by CTR. Top is the frequency domain characterization, bottom is the time-domain characterization (inverse Fourier transform of the frequency characteristics). A single 802.11a WiFi channel bandwidth is indicated on the frequency chart for comparison with the 2.40 to 2.48 ISM band (frequency band measurement).

Finally, a noise RADAR operating around a 4.3 GHz carrier demonstrates the feasibility of this approach with

WAIC emitters expected to fit future aircrafts. In this case, the classical SAW delay line becomes unsuitable due to excessive lithography resolution requirements and surface wave propagation losses. Our demonstration focuses on using the High-overtone Bulk Acoustic Resonator as cooperative target compatible with such a high frequency.

II. From noise RADAR to passive RADAR

The range resolution of a RADAR is inversely proportional to the emitted signal bandwidth. Multiple strategies are available for spreading a carrier: generating short pulses inducing a broadband spectrum (pulsed RADAR), sweeping the carrier frequency and collecting the scattering coefficient at each frequency (Frequency Stepped Continuous Wave), linearly sweeping the carrier frequency and measuring the beat signal with the returned echoes (the beat signal frequency being then proportional to the echo delay – Frequency Modulated Continuous Wave) or pseudo-random phase modulation of the carrier. We are interested here in the latter, classically used in Code Division Multiple Access (CDMA) communication such as the Global Navigation Satellite (GPS) system. An attractive feature of the Binary Phase Shift Keying (BPSK) modulation is its simplicity: a mixer fed on its local oscillator port with the carrier signal and on its intermediate frequency port by a digital signal defining the pseudo-random sequence will generate on the radiofrequency port a spread spectrum signal with a bandwidth defined by the bit-rate of the pseudo-random digital sequence and a center frequency defined by the carrier (Fig. 2).

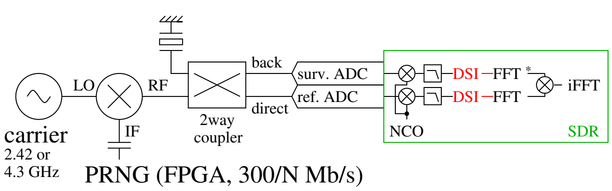

Fig. 2. Noise RADAR demonstration architecture. The wireless link is replaced by a 2-way coupler, with the sensor connected to the output port. The coupled output feeds the reference channel analog-to-digital (ADC) converter, the reverse channel feeds the surveillance channel including the sensor response. The Numerically Controlled Oscillator (NCO), low pass filter, possibly Direct Signal Interference identification and removal, and cross-correlation as the inverse Fourier transform of the product of the Fourier transform of the reference signal times the complex conjugate of the Fourier transform of the surveillance signal, are all implemented as software.

Results shown in this paper for noise RADAR focus on a wired connection between the sensor and the coupler to demonstrate the concept of the noise RADAR approach. This strategy is nevertheless well suited for a wireless characterization of the SAW response, as was shown in [1] in which a bistatic range beyond 1 m was achieved with this basic setup.

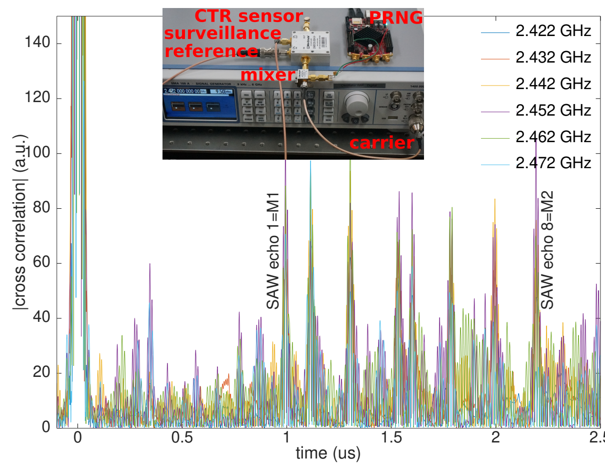

Fig. 3. Noise RADAR measurement of a 2.4 GHz CTR delay line. A frequency synthesizer generates the carrier frequency from 2.422 to 2.472 GHz with 10 MHz steps, while a pseudo-random generator (PRNG) running at 37.5 Mb/s switches the phase by polarizing the intermediate frequency input of the mixer, spreading the carrier. A ZABDC20-252H bi-directional coupler provides the coupled output (reference channels) and the reverse output (sensor output) used as surveillance channel, both feeding two channels of a LeCroy MCM-Zi-A radiofrequency grade oscilloscope sampling at 5 GS/s. The 8 echoes ranging from 1.0 to 2.2 μs delay are well visible on the cross-correlation magnitude. SAW echo markers M1 and M2 refer to the time characterization shown in Fig. 1 (bottom).

However, the radiofrequency is a scarce resource, and emitting is strongly regulated. Not only are the duty cycle, mean power and maximum power defined in the regulations, the field of application must be met as well: few, if any, frequency bands allow short range RADAR system emissions. We here address the regulatory issue of emitting short range RADAR signals by using existing emission sources: the underlying principle of the passive RADAR approach is to select a source random enough for the pseudo-random assumption to be met, yielding a correlation function close to a Dirac function distributed along the echo delays. Too correlated signal sources will spread the correlation peak and prevent nearby target separation. Since the non-cooperative emitter signal is not known, a passive RADAR is classically designed as a bistatic RADAR, with one antenna monitoring the reference signal and another antenna monitoring the reflections from targets: the so called reference and surveillance antennas.

Since RADAR signals decay as the fourth power of the range, powerful emitters must be selected: all radiofrequency sources have been investigated for passive RADAR applications, including analog television now replaced with digital television, commercial broadcast frequency modulated emissions, digital audio broadcast, mobile phones or microwave emissions such as IEEE 802.11 (WiFi) transceivers.

III. Passive RADAR for passive sensor measurement

RADAR targets are usually considered as broadband reflectors, returning a signal at all wavelengths shorter than the typical dimensions of the target. Here we are interested in designing cooperative targets for passive RADAR applications: these targets not only return echoes related to the presence of the target, but the delays encode an information. In case of an identification code the target is called a tag, and if the delay is dependent on a physical quantity, the target is called a sensor. Cooperative targets classically include resonant cavities (e.g. Leon Theremin's passive microphone [2]), dielectric resonator, or delay line [3].

Shrinking cooperative target dimensions is classically achieved by converting the electromagnetic wave to the 10^5 times slower acoustic wave using the electromechanical conversion capability of piezoelectric substrates [4]. Hence, the meter long dielectric delay lines shrink to millimeter acoustic delay lines by patterning interdigitated electrodes and mirrors on a piezoelectric substrate. Furthermore, the acoustic velocity dependence with the physical environment of the piezoelectric substrate – temperature, stress, boundary conditions for chemical sensors – intrinsically confers sensing capability to such a device. However, the relative operating bandwidth of acoustic transducers is given by the electromechanical coupling coefficient, usually a few percents at most. Hence, the passive RADAR interrogation of acoustic transducers requires a closer match between the spectrum emitted by the non-cooperative target and the transducer transfer function. In the demonstrations addressed in this article, we tackle two wireless protocols available in planes: IEEE 802.11 (WiFi) and WAIC. The former frequency band, 2.40 to 2.48 GHz, is readily accessible with commercial, off the shelf acoustic delay lines as provided by RSSI Gmbh (Germany) and CTR (Austria). The latter frequency band, from 4.2 to 4.4 GHz, is hardly accessible to surface acoustic wave delay lines, and will be the opportunity to introduce an alternative cooperative sensor geometry, namely the High-overtone Bulk Acoustic Resonator (HBAR) whose operating frequency is no longer limited by a lithography resolution criterion but by a thin piezoelectric film deposition thickness [5].

IV. Passive RADAR interrogation in the 2.4 GHz WiFi band

The non-cooperative source is a USB-WiFi dongle configured in monitoring mode so as to continuously stream data even if not associated with an access point. As a first demonstration, the carrier frequency is set to channel 3 centered on 2.422 GHz, within the sensor bandpass. The WiFi dongle is set to monitor mode to continuously stream packets, yet with a reduced bandwidth of 15 MHz, providing after cross-correlation a 67 ns resolution, below the typical 100 ns time delay between adjacent echoes from acoustic sensor responses. Nevertheless as a second demonstration, the time resolution is improved by scanning multiple adjacent WiFi channels and combining the data to increase bandwidth and hence improve the timing resolution: scanning from channel 1 to 11 or 2.412 to 2.462 GHz provides, in addition to the 15 MHz bandwidth of each channel, a total bandwidth of 65 MHz and hence a timing resolution of 15 ns, allowing for the separation of multiple sensors communicating in the same frequency band but using Time Division Multiple Access (TDMA) by returning echoes delayed by different values for each sensor.

The local oscillator LO used for down-conversion of the radiofrequency signal is on purpose shifted by 60 MHz to not cover the WiFi frequency band. Indeed, WiFi monitors the received power at the operating frequency, and the LO signal leaked through the coupler and mixer will be enough to make the WiFi dongle drop connection if a signal is detected within the operating range. Hence, the sampling frequency is set to 250 MHz, sufficiently broadband to include all 802.11 channels and the frequency offset introduced by LO set to 2.48 GHz. During post-processing, the 60 MHz offset is removed using a software implementation of the local oscillator and mixer (multiplication) to bring the signal back to baseband with a slowly varying stable phase information as needed to extract finely the time delay and hence the physical quantity under investigation.

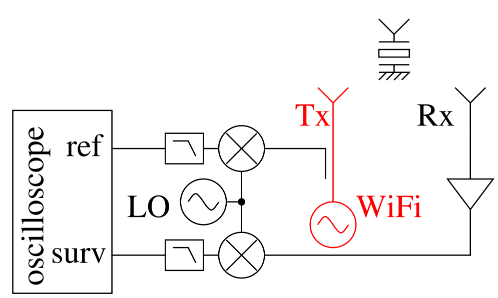

Fig. 4. Schematic of the experimental setup.

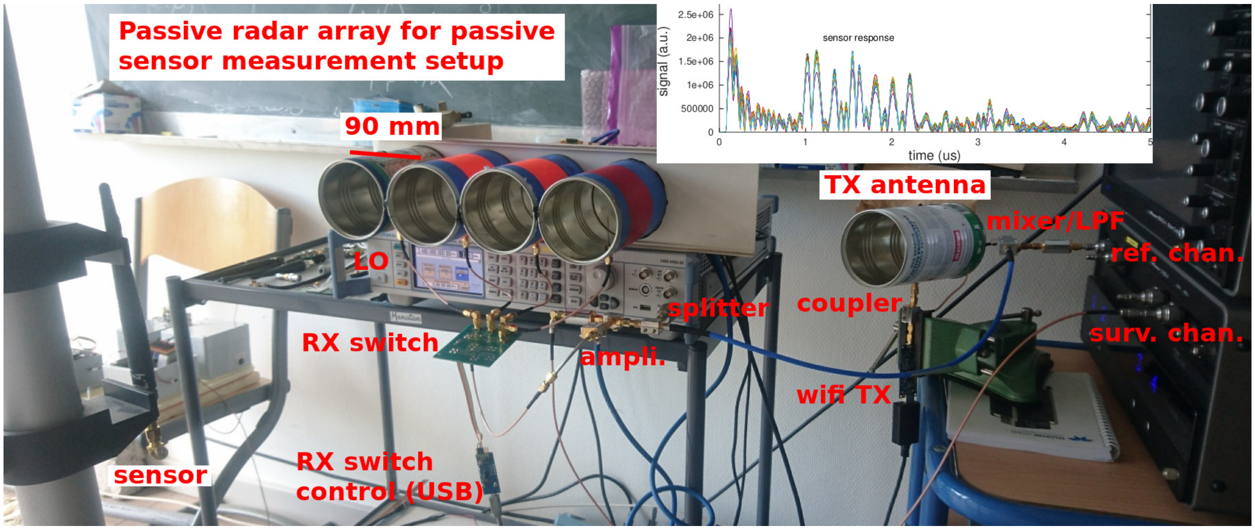

Fig. 5. Picture of the experimental setup. For scale, each cantenna is 90 mm-diameter. Inset: result of 20 successive measurements separated by 2.24 s, demonstrating the consistency of the analysis. The 8-bit sensor response is visible at delays ranging from 1.0 to 2.2 μs (sensor provided by CTR). The correlation peaks close to 3.2 μs are due to the intrinsic IEEE 802.11 (WiFi) signal properties.

All data are collected on two synchronous channels of a digital oscilloscope, one collecting the reference signal directly coupled from the WiFi emitter and down-converted using a mixer whose local oscillator is fed by the 2.48 GHz LO signal followed by a 190 MHz low pass-filter, and the other collecting the down-converted and similarly filtered surveillance channel. In order to further investigate direction of arrival (or synthetic aperture) processing, the single surveillance antenna is replaced with an array of 4 cantennas separated by 90 mm and fed by a radiofrequency switch (Hittite HMC241, now Analog Devices). A personal computer synchronizes the switch configuration as defined by a USB to GPIO converter (FTDI FT232) and the data collection from the digital oscilloscope for post-processing. For each new antenna setting, both reference and surveillance channel data are collected and stored (Fig. 5).

A. Signal identification

A real signal, as emitted by WiFi, is not random but presents some structure repeated over time: the correlation is not a Dirac function but is spread over a duration spanning multiple microseconds. Despite the sensor design aimed at separating the sensor delay from clutter, the autocorrelation of WiFi is too broad to recover the minute returned power from the sensor. As seen on Fig. 6, the Direct Signal Interference (DSI) overwhelms the sensor response (blue). In a wireless configuration, subtracting the direct signal (reference channel) from the sensor measurement (surveillance channel) as identified by a least square algorithm is not sufficient since time delayed copies of the reference signal bouncing on surrounding obstacles with cross sections much larger than the sensor returned power have been recorded. Thus, time delayed copies of the reference channel must be subtracted as well, until the sensor response appears: a tradeoff between computational power requirement and maximum delay defines the size of the matrices handled during the least square weight estimation of each delayed reference signal copy. Fig. 6 demonstrates that subtracting delays of 60 ns maximum (15 sample-delays when sampling at 250 MS/s) is sufficient, and increasing the delay to 160 ns does not improve the ability to extract the sensor information. In all cases, the delay must remain below the 1 μs at which the first sensor echo is located.

A single WiFi channel spans 15 MHz, allowing for a delay resolution of about $1000/15 = 67$ ns. While sufficient for separating echoes delayed by more than 100 ns, the timing resolution defines the number of bits that can be included in the 80 MHz wide 2.4 GHz Industrial, Scientific and Medical (ISM) band. Improving the time resolution is achieved by successively probing the sensor response in multiple WiFi channel carrier frequencies. Since the local oscillator and sampling frequency are not changed from one measurement to another, combining these measurements is achieved by summing the Fourier transforms, as long as the sampling frequency is high enough for each measurement to cover all the channels. The time resolution improvement is illustrated in Fig. 7.

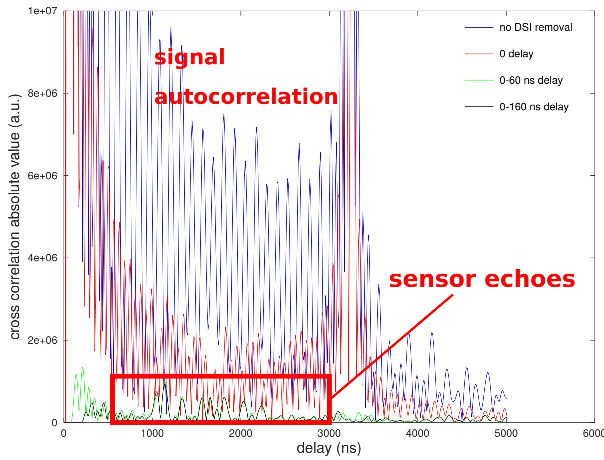

Fig. 6. Direct Signal Interference subtraction: 0-delay DSI subtraction is not sufficient to detect the echoes, but removing the first 6-sample delayed echoes reduces DSI below the sensor response.

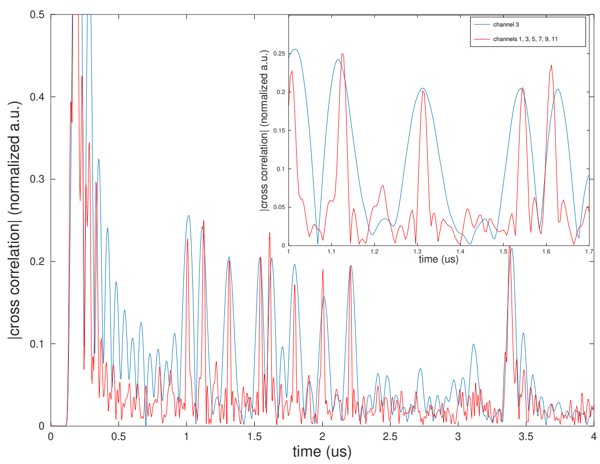

Fig. 7. Single channel measurement (blue) and broadband measurement (red) achieved by aggregating measurements collected on WiFi channels 1 to 11. The autocorrelation peak at 3.2 μs width is not affected by the broader bandwidth measurement, while the acoustic sensor echoes become sharper as bandwidth is increased.

B. Measurement extraction

Cross correlation is a linear process so that phase of the returned signal is representative of the time delay between the reference signal and the surveillance signal. While in a broadband reflector (target) the time delay is solely defined by the time of flight of the electromagnetic wave from source to target and target to receiver, the cooperative target introduces an additional delay as the acoustic propagation delay of the surface acoustic wave on the sensor. Thus, each echo phase includes two informations, the electromagnetic time of flight added to the acoustic time of flight. The former is solely defined by the bistatic range, while the latter is solely defined by the acoustic sensor geometry and the acoustic velocity, the latter quantity being dependent on the physical quantity under investigation, in our case temperature since the piezoelectric substrate used – YXl/128° lithium niobate – exhibits a large, $S = 60$ ppm/K, temperature sensitivity. By subtracting the phase from two echoes returned by the sensor as monitored by a single antenna, the electromagnetic time of flight contribution is cancelled – assuming the sensor has not moved during the measurement – and only the acoustic delay representative of the temperature remains. One challenge in using the phase to recover the physical quantity if the 2π phase rotation introduced for large physical quantity variations. For a time delay τ and a center operating frequency f, the phase φ introduced by the acoustic wave propagation is $\varphi = 2\pi f \tau$ so that a 2π phase rotation due to temperature variation ΔT is observed if $\Delta T = (Sf\tau)^{-1}$. If a temperature range of 100 K is considered at an operating frequency of 2.42 GHz, then the delay should be no longer than 69 ns. Two of the echoes returned by our sensor are separated by 84 ns, allowing for a measurement on such a large temperature range without 2π phase rotation (Fig. 8).

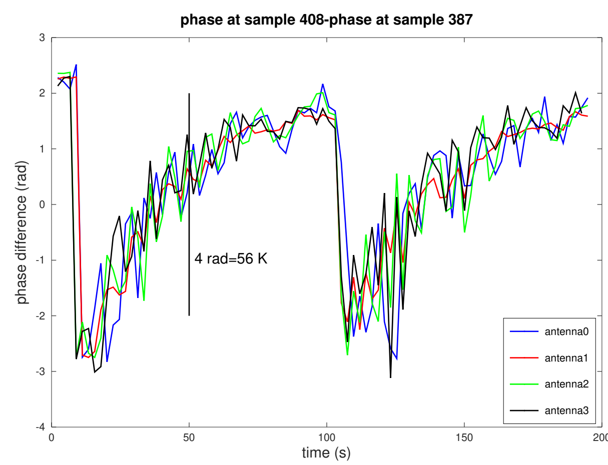

Fig. 8. Temperature measurement using one sensor illuminated by a single non-cooperative emitter and with four surveillance antennas. Subtracting two echo phases gets rid of the sensor to antenna distance and the remaining phase information is solely representative on the acoustic velocity, dependent on the temperature. Here the sensor was cooled twice using a freezing spray around 10 and 100 s. The measurement is at the threshold of the interrogation range, at 1.2 m bistatic range (75 cm from emitter to sensor and 45 cm from sensor to receiver) using the cantennas, hence the poor signal to noise ratio with respect to the result shown in Fig. 9.

1) Temperature measurement accuracy assessment:

A passive wireless SAW sensor is fitted with a reference Pt100 temperature probe and heated by a power resistor glued to the package. One measurement example, given in Fig. 9, exhibits at a bistatic range of 1 m (60 cm from source to sensor and 40 cm from sensor to surveillance antenna), a standard deviation on the temperature measurement of 0.1 K in the initial stage when no heating is applied. The match between the reference probe temperature variation and the SAW sensor response is achieved by selecting a temperature sensitivity of -76 ppm/K, well within tabulated value ranges [4] of the temperature sensitivity of (YXl)/128° lithium niobate. The time delay between the SAW sensor response and the Pt100 probe is attributed to the different thermal inertia between the bulkier TO39 packaged SAW sensor and the high thermal resistance of the piezoelectric substrate with respect to the smaller Pt100 sensing element.

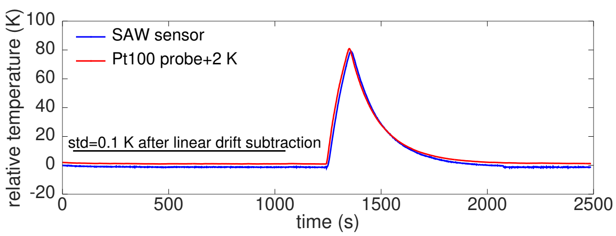

Fig. 9. Top: raw cross-correlation phase measurement of the first echo located at 1 μs delay as the sensor is heated twice. The measurement is performed at a bistatic range of 1 m. Bottom: conversion of phase to temperature using the tabulated -76 ppm/K temperature sensitivity of (YXl)/128° lithium niobate, overlapped with the measurement from a reference Pt100 temperature probe. The reference temperature is offset by 2 K to make the two curves easier to see. The thick horizontal line, spanning from 50 to 1050 s, indicates the duration over which the standard deviation (std) on the temperature measurement following the removal of the linear drift (0.1 K over 1000) due to the leftover cooling of the sensor from the previous experiment.

In this experiment, the directional emitting and receiving cantennas were replaced with circularly polarized Huber&Suhner (Switzerland) SPA-2400/70/9/0/LCP patch antennas, yielding improved signal to noise ratio in addition to a shorter bistatic range with respect to the measurement exhibited in Fig. 8.

V. Beyond WiFi (2.40–2.48 GHz): WAIC (4.2–4.4 GHz)

Surface acoustic wave devices operating frequency range is limited by acoustic losses. Indeed, acoustic losses scale quadratically with frequency, and in addition to manufacturing challenges (small lithography dimensions), reaching the WAIC 4.2 GHz becomes challenging for a practical use of SAW devices. On the other hand, bulk acoustic resonators do not exhibit limitation due to lithography process, but to thin film deposition process. One technology demonstrating promising performance for filling the gap between compact, acoustic radiofrequency SAW devices (100–2500 MHz) and dielectric resonators (10 GHz and above) is the High-overtone Bulk Acoustic Resonator (HBAR) architecture. In this device, a thin piezoelectric film coats a low loss acoustic substrate: the piezoelectric film acts as an energy pump to fill the reservoir made of the low loss acoustic substrate, providing additionally a rugged architecture. Because the HBAR provides multiple modes separated by a delay given by the the substrate thickness to acoustic velocity ratio, the comb of modes in the frequency domain is analyzed here, through a Fourier transform, as a comb of modes in the time domain. The periodic echoes, delayed by a duration dependent on the acoustic velocity and hence the physical quantity under investigation, is ideally suited for a delay line interrogation scheme as presented earlier [6].

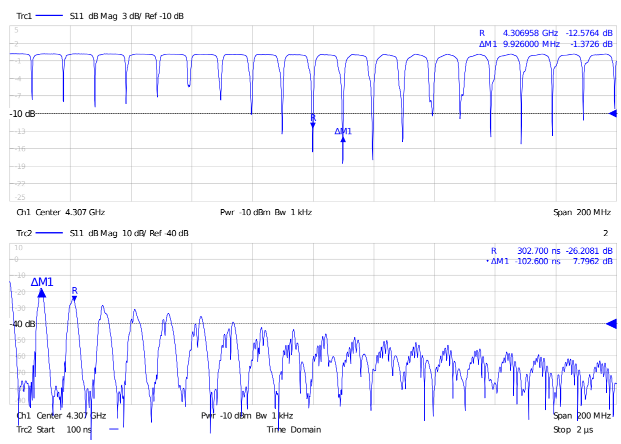

Fig. 10. Reflection scattering coefficient of the HBAR operating at 4.3 GHz.

Due to the lack of a WAIC emitter to demonstrate the passive RADAR approach, we use a pseudo random generator to spread a 4.3 GHz carrier and demonstrate the suitability of the passive RADAR strategy even for such high microwave frequencies as those used in the aeronautical standard. The target HBAR exhibits a comb of modes spaced by 10 MHz, whose inverse Fourier transform yields a set of echoes separated by 100 ns. The pseudo-random sequence runs as 150 MHz to probe multiple modes: the first two echoes delayed by the cooperative target are exhibited in Fig. 11, allowing for a differential time of flight measurement insensitive to the RADAR to sensor distance.

This experiment is completed by connecting the pseudo-random generator to the intermediate frequency input of a MiniCircuits ZX05-C60LH-S+ mixer whose local oscillator is connected to a 4.3 GHz source and output feeds the input of a MiniCircuits SYBD-13-63HP+ bidirectional coupler. The HBAR sensor is connected to the output of the coupler, the forward coupled output provides the reference signal and the reverse coupled output the surveillance channel.

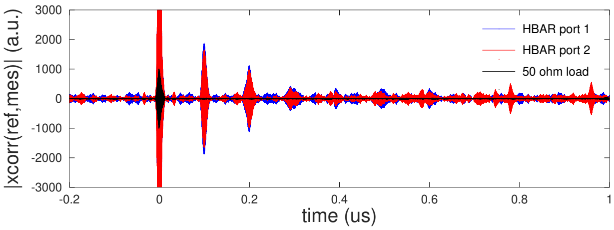

Fig. 11. HBAR interrogation using a noise RADAR spreading a 4.3 GHz carrier to a 150 MHz bandwidth. The responses of two HBAR located nearby on the wafer are compared to demonstrate the reproducibility of the measurement and emphasize the relevance of the measurement with respect to the response recorded in absence of the sensor.

A temperature measurement capability assessment is completed by collected the reference and surveillance signals from the bidirectional coupler while the HBAR, which has been glued using heat-conducting epoxy to a power resistor to which a reference Pt100 probe was also fitted, is heated and then cooled. The first echo delay is precisely located by performing a second-order polynomial fit on the echo maximum and recording the parabola maximum position. Since an HBAR is a stack of heterogeneous substrates, predicting the temperature sensitivity is a more complex task than in the case of the delay line patterned on the single crystal lithium niobate substrate. Here the echo delay has been scaled to match the temperature excursion observed from the reference Pt100 probe, exhibiting excellent match of the thermal kinetics as observed with both sensors (Fig. 12).

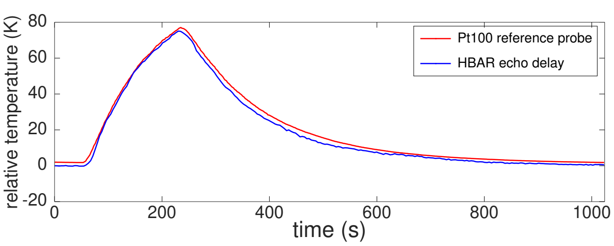

Fig. 12. Simultaneous measurement of the temperature of a heating resistor measured by a reference Pt100 probe and through the time delay of the first echo from an HBAR probed by the noise radar. For clarity, the Pt100 temperature has been raised by 2 K to separate the two curves.

VI. Spatial separation of sensor responses

Having provided a solution to radiofrequency regulations for probing SAW sensors, we tackle a second issue in SAW delay line deployment, namely sensor response collision. Indeed, if multiple sensors are exposed to the non-cooperative source illumination, their linear responses induces a series of delayed echoes, the vectorial sum of which is recovered by the receiver. Various mitigation strategies are available such as Time Division Multiple Access (TDMA) in which echoes are delayed by different times for each sensor, or Frequency Division Multiple Access (FDMA) in which each sensor transfer function is located in different frequency bands. These strategies require that in a given environment, no two similar sensors are simultaneously seen by the non-cooperative source and the receiver.

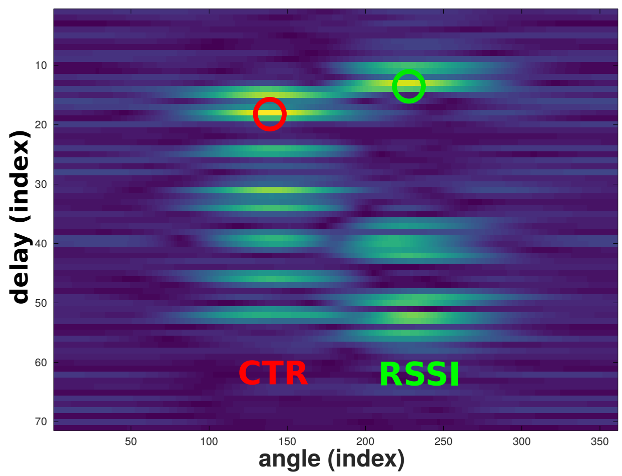

Fig. 13. Range-azimuth map of two sensors – one provided by CTR, the other one by RSSI – illuminated by a WiFi non-cooperative emitter and whose signal is collected by an 8-dipole uniformly-spaced linear receiving array. A Fourier transform along the azimuthal angle axis allows for spatially separating the two contributions even though the far field condition is hardly met. The two circles annotated with the supplier name indicate which echo phase is analyzed for temperature extraction.

Here we introduce Spatial Division Multiple Access (SDMA) by replacing the unique receiving antenna by a uniformly-spaced linear array (ULA). Under the assumption that the sensor is located in the far field region so that the array is illuminated by a plane wave, and assuming that the antennas in the array are uniformly spaced, then the same phase offset is introduced between adjacent antenna signals. Focusing the signal back to the incoming direction angle (azimuth) is expressed as a Fourier transform along the azimuth axis as shown in [7] (Fig. 13).

With respect to this reference, we here show that the linear Fourier transform along the azimuth axis keeps the phase information and hence allows for recovering the temperature information, in addition to being robust to the far field condition which is hardly met in our experimental setup (Fig.14). Indeed, with dipole antenna separation of $\lambda/2 = 6.2$ cm, then the far field condition

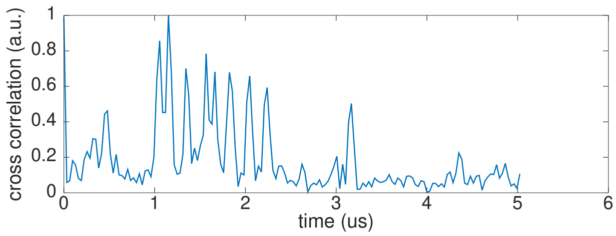

Fig. 14. Cross section of the range-azimuth map at index 149 along the azimuth (Fig. 13), exhibiting the magnitude of the returned signal along the direction of arrival of the signal returned by the CTR sensor. The eight successive echoes are well visible on this chart.

assumes a range of $R_0 \gg L^2/\lambda$ with L the array length – in our case the 8-antenna receiving array is $7 \times \lambda/2 = 43$ cm long so that $R_0 \gg 3$ m or 6 m bistatic range, well beyond our current operating setup geometry. Nevertheless, the Fourier transform along the azimuth allows for separating adjacent sensor contributions, and by analyzing the phase of echoes thus separated, to recover each temperature information (Fig. 15).

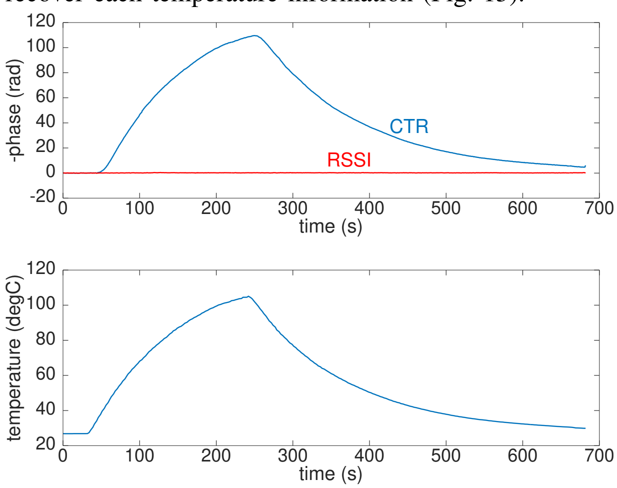

Fig. 15. Top: phase of the heated CTR sensor (blue) and phase of the RSSI sensor kept at room temperature during the experiment. Bottom: temperature record from the reference Pt100 probe glued to the power resistor glued to the CTR sensor. The ability to separate the temperature from the various sensors is hence demonstrated in addition to azimuthal separation of the responses.

Fig. 15 hence demonstrates our ability to select the echo representative of one single sensor, extract its phase, and recover the temperature of the (CTR) heated sensor while observing that the other (RSSI) sensor kept at room temperature during the experiment does not exhibit a visible phase change due to signal processing artifacts.

VII. Conclusion

We have tackled the issue of certification of the passive acoustic sensor wireless measurement electronic system by addressing the ability of a passive RADAR approach to recover the fine echo delay and extract the physical quantity causing a change in the acoustic velocity. Having demonstrated the concept using a dedicated noise RADAR for spreading the 2.4 GHz carrier, we have used a WiFi emitter as radiofrequency source to illuminate the sensor target: direct signal interference removal and cross correlation of the (coupled) reference signal and reference signal allow for recovering, through the phase of the cross-correlation, a fine estimate of the echo delay difference solely dependent on the acoustic velocity and hence the physical quantity measurement. The demonstration has been extended to a noise RADAR applied to another acoustic sensor architecture, the High-overtone Bulk Acoustic Resonator, suitable to operate in the 4.3 GHz aeronautical WAIC band. Finally, the collision issue of multiple sensors simultaneously illuminated by the non-cooperative emitter whose signals are detected by the passive radar receiver is addressed: this issue is solved by replacing the single receiving antenna with an array allowing for synthetic aperture analysis and spatially separating the contribution of each sensor.

Acknowledgements

B. Bloessl, author of `gr-ieee802-11` at https://github.com/bastibl/gr-ieee802-11, provided the explanation and scripts for setting the WiFi emitter to monitor mode to continuously stream data and illuminate in a reproducible way the cooperative targets. The HBAR transducer was fabricated by CEA LETI (Grenoble, France) in the framework of the ORAGE project. Tohoku University (Sendai, Japan) provided a visiting scientist grant to J.-MF prompting this investigation. S.-E. Hamran introduced noise RADAR to J.-MF.

References

[1] W. Feng, J.-M. Friedt, G. Goavec-Merou, and M. Sato, "Passive radar delay and angle of arrival measurements of multiple acoustic delay lines used as passive sensors," *IEEE Sensors*, vol. submitted, 2018.

[2] A. Glinsky, *Theremin: ether music and espionage*. University of Illinois Press, 2000.

[3] C. Allen, K. Shi, and R. Plumb, "The use of ground-penetrating radar with a cooperative target," *IEEE Transactions on Geoscience and Remote Sensing*, vol. 36, no. 5, pp. 1821–1825, 1998.

[4] D. Morgan, "Surface acoustic wave filters," *Amsterdam: Elsevier*, 2007.

[5] A. Reinhardt *et al.*, "Ultra-high qf product laterally-coupled AlN/silicon and AlN/sapphire high overtone bulk acoustic wave resonators," in *IEEE International Ultrasonics Symposium (IUS)*. IEEE, 2013, pp. 1922–1925.

[6] J.-M. Friedt *et al.*, "High-overtone bulk acoustic resonator as passive sensor acting as buried cooperative target interrogated by ground penetrating RADAR," in *IEEE International Frequency Control Symposium (IFCS)*, Prague, Czech Rep., 2013.

[7] W. Feng, J.-M. Friedt, G. Goavec-Merou, and M. Sato, "Passive radar delay and angle of arrival measurements of multiple acoustic delay lines used as passive sensors," *IEEE Sensors*, 2018, submitted.